A&A 409, 1141–1149 (2003)
DOI: 10.1051/0004-6361:20031184


Astronomy & Astrophysics

# Improved oscillator strengths and wavelengths for Os I and Ir I, and new results on early *r*-process nucleosynthesis⋆

S. Ivarsson[1], J. Andersen[2,3], B. Nordström[1,2], X. Dai[4], S. Johansson[1], H. Lundberg[4], H. Nilsson[1], V. Hill[5], M. Lundqvist[1], and J. F. Wyart[6]

[1] Atomic Astrophysics, Lund Observatory, Lund University, PO Box 43, 22100 Lund, Sweden
[2] Astronomical Observatory, Niels Bohr Institute for Astronomy, Physics & Geophysics, Juliane Maries Vej 30, 2100 Copenhagen, Denmark
[3] Nordic Optical Telescope Scientific Association, La Palma, Canary Islands, Spain
[4] Atomic Physics, Department of Physics, Lund Institute of Technology, PO Box 118, 22100 Lund, Sweden
[5] GEPI, Observatoire de Paris-Meudon (UMR 8111), DASGAL, 2 pl. Jules Janssen, 92195 Meudon Cedex, France
[6] Laboratoire Aimé Cotton, Centre National de la Recherche Scientifique, Orsay, France

Received 28 May 2003 / Accepted 25 July 2003

**Abstract.** The radioactive decay of $^{238}$U and $^{232}$Th has recently been used to determine ages for some of the oldest stars in the Universe. This has highlighted the need for accurate observational constraints on production models for the heaviest *r*-process elements which might serve as stable references, notably osmium and iridium. In order to provide a firmer basis for the observed abundances, we have performed laser-induced fluorescence measurements and Fourier Transform Spectroscopy to determine new radiative lifetimes and branching fractions for selected levels in Os I and Ir I. From these data, we determine new absolute oscillator strengths and improved wavelengths for 18 Os I and 4 Ir I lines.
A reanalysis of VLT spectra of CS 31082-001 and new results for other stars with Os and Ir detections show that (i): the lines in the UV and $\lambda$ 4260 Å yield reliable Os abundances, while those at $\lambda\lambda$ 4135, 4420 Å are heavily affected by blending; (ii): the Os and Ir abundances are identical in all the stars; (iii): the heavy-element abundances in very metal-poor stars conform closely to the scaled solar *r*-process pattern throughout the range $56 \leq Z \leq 77$; and (iv): neither Os or Ir nor any lighter species are suitable as reference elements for the radioactive decay of Th and U.

**Key words.** atomic data – nuclear reactions, nucleosynthesis, abundances – stars: abundances – stars: individual: CS 31082-001

## 1. Introduction

Very metal-poor halo stars with greatly enhanced abundances of the heaviest neutron-capture elements have recently been identified (Sneden et al. 1996; Hill et al. 2002). These stars are of particular interest for two reasons: (i) their heavy elements were produced by the *r*-process in a very small number ($\geq$1) of supernovae or similar violent progenitor events in the first generation of stars in the Galaxy (and in the Universe); and (ii) the abundances of the *r*-process elements can be accurately determined, due to the negligible interference from lines of iron-peak elements. Interest in these stars was greatly heightened by the recent discovery of uranium in the very metal-poor star CS 31082-001 (Cayrel et al. 2001), which opened the way to a new, accurate and fundamental method to determine the age of such ancient stars by radioactive dating.

Testing theoretical models for the explosive nucleosynthesis of the heaviest elements, especially as regards their application to radioactive cosmochronology, places strong demands on the atomic parameters used to convert measured stellar line strengths into accurate absolute abundances. Os and Ir are of special interest in this context: These are among the heaviest stable elements that can be observed in metal-poor stars in the optical region and thus potentially more reliable reference elements for the decay of the radioactive species $^{238}$U and $^{232}$Th than Eu. $^{232}$Th/$^{151}$Eu was used in conventional Th/Eu chronometry, but its initial production ratio is now known to be affected by large uncertainties (Wanajo et al. 2002; Schatz et al. 2002). However, Os and Ir also serve to define the limit in atomic mass below which the *r*-process elements appear to be produced in constant proportions; above this limit, at least such actinides as Th and U have a component of different origin (Hill et al. 2002; Johnson & Bolte 2002).

*Send offprint requests to*: S. Ivarsson,
e-mail: stefan.ivarsson@astro.lu.se

⋆ Based in part on observations obtained with the Very Large Telescope of the European Southern Observatory at Paranal, Chile.

Accurate abundances of Os and Ir are therefore of great significance, both in radioactive cosmochronology and as constraints on the structure, variety, and nucleosynthetic yields of supernovae from the first stellar generation. This motivated us to undertake a new determination of oscillator strengths for the astrophysically most important lines of Os I and Ir I. We also redetermine the Os and Ir abundances in CS 31082-001 from an expanded set of lines, reaching significant new conclusions on the production of these elements in the first stars.

## 2. Laboratory data for Os I and Ir I

Experimental oscillator strengths for neutral osmium (Os I) were first reported by Corliss & Bozman (1962). Later, Kwiatkowski et al. (1984) measured lifetimes for six energy levels, which they used to rescale and adjust some of the $f$-values of Corliss & Bozman. For neutral iridium (Ir I), experimental oscillator strengths for 27 lines were determined by Gough et al. (1983). They combined radiative lifetimes, measured by a laser-excitation fluorescence technique, with experimental branching fractions obtained from spectra of a Ne-Ir hollow-cathode lamp recorded with an intensity-calibrated monochromator.

In this paper we present radiative lifetimes of four levels of Os I and one level of Ir I, measured at the Lund Laser Centre (LLC) by means of the laser-induced fluorescence (LIF) technique. We also report branching fractions, determined with the Lund UV Fourier Transform Spectrometer (FTS), for transitions from six Os I levels and two Ir I levels. Combining all these new data and one previously measured lifetime for each of Os I and Ir I (Gough et al. 1983; Kwiatkowski et al. 1984), we derive new oscillator strengths for 18 Os I and 4 Ir I lines in the wavelength region 2900–5100 Å. For all the transitions measured we also present improved centre-of-gravity wavelengths.

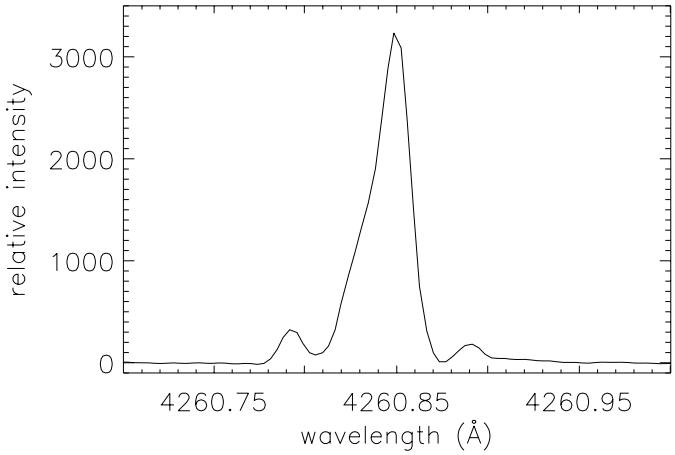


**Fig. 1.** Observed line structure for the $5d^6 6s^2\ {}^5D_4 - 5d^6 6s(^6D)6p\ z\ {}^7D_5$ transition of Os I observed at 4260.849 Å in the laboratory FTS spectrum.

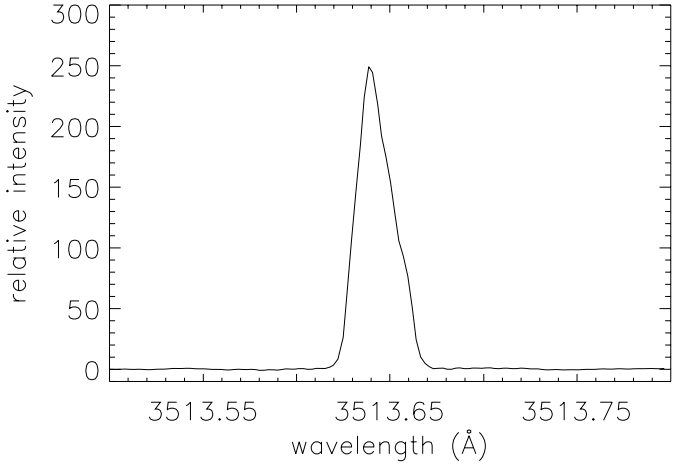


**Fig. 2.** Unresolved structure of the $5d^7 6s^2\ a^4F_{9/2} - 5d^7 6s(^5F)6p\ z^6F_{11/2}$ transition of Ir I observed at 3513.6473 Å in the laboratory FTS spectrum.

## 3. Atomic properties and structure of Os I and Ir I

### 3.1. Osmium

Osmium has seven stable isotopes with the mass numbers and relative terrestrial abundances $A$ = 184 (0.02%), 186 (1.6%), 187 (1.6%), 188 (13.3%), 189 (16.1%), 190 (26.4%) and 192 (41.0%) (Kröger et al. 2002). The even isotopes, which account for more than 80% of all osmium, have no hyperfine structure (hfs). Nevertheless, a weak blue-shifted hfs component is seen for some of the strongest transitions, resolved from the main spectral feature (see e.g. $\lambda$4260 in Fig. 1). The red-shifted component, resolved in Fig. 1, is due to the isotope shift of the isotopes $A$ = 188 and $A$ = 189. The $A$ = 184, 186 and 187 isotopes have too low abundances to be observed.

The main spectral feature in Fig. 1 is asymmetric due to the unresolved blend of the two most abundant isotopes, $A$ = 190 and 192, and is thus affected by isotope shift. The extensive study by Kröger et al. (2002) used laser induced fluorescence spectroscopy to resolve and measure the hyperfine structure and isotope shifts of numerous levels and lines in Os I.

The ground state and the lowest levels of Os I belong to the even-parity configurations $5d^6 6s^2$ and $5d^7 6s$ (Van Kleef & Klinkenberg 1961). The lowest configurations of odd parity, $5d^6 6s6p$ and $5d^5 6s^2 6p$, appear around 3 eV. The transition arrays between these two sets of levels represent the strongest lines in the Os I spectrum, and they appear in the wavelength region 2500 to 4500 Å.

### 3.2. Iridium

Iridium has two stable isotopes, $A$ = 191 and 193, with relative terrestrial abundances of 37.3% and 62.7%. The asymmetric features in the FTS spectrum are unresolved blends of hyperfine structure and/or isotope shift components, as shown by the example in Fig. 2. A detailed analysis of the hyperfine structure and isotopic shift in Ir I has been published by Sawatzky & Winkler (1989), who studied these effects by means of optical interference spectroscopy.

**Table 1.** Experimental radiative lifetimes of four levels in Os I.

| Level[a] | Energy ($cm^{-1}$) | $J$ | $\lambda^b_{exc}$ (Å) | $\lambda^c_{obs}$ (Å) | Lifetime (ns): Exp[d] This work | K | CB |
|---|---|---|---|---|---|---|---|
| $5d^56s^2(^6S)6p\ z\ ^7P_4$ | 28 331.736 | 4.0 | 4311.3 | 4135 | 265(20) | 238.0(12) | 70.2 |
| $5d^66s(^6D)6p\ z\ ^7F_5$ | 30 279.921 | 5.0 | 3301.5 | 3977 | 93 (7) | 91.0 (5) | 27.5 |
| $5d^66s(^6D)6p\ z\ ^7F_4$ | 32 684.629 | 4.0 | 3058.6 | 3504 | 28 (2) | 27.3 (2) | 9.6 |
| $5d^66s(^6D)6p\ z\ ^5F_5$ | 34 365.335 | 5.0 | 2909.0 | 2909 | 24 (2) | | |

[a] Level notation from Van Kleef & Klinkenberg (1961).
[b] Laser wavelength used to populate the upper state.
[c] Wavelength used to detect the fluorescence signal.
[d] K = Kwiatkowski et al. (1984), CB = Corliss & Bozman (1962).

**Table 2.** Experimental radiative lifetimes of two levels in Ir I.

| Level[a] | Energy ($cm^{-1}$) | $J$ | $\lambda^b_{exc}$ (Å) | $\lambda^c_{obs}$ (Å) | Lifetime (ns): Exp[d] This work | G |
|---|---|---|---|---|---|---|
| $5d^76s(^5F)6p\ z\ ^6F_{11/2}$ | 28 452.32 | 5.5 | 3513.6 | 3902 | 320(30) | 340(10) |
| $5d^76s(^5F)6p\ z\ ^6D_{9/2}$ | 26 307.49 | 4.5 | | | | 580(10) |

[a] Level notation from Van Kleef (1957).
[b] Laser wavelength used to populate the upper state.
[c] Wavelength used to detect the fluorescence signal.
[d] G = Gough et al. (1983).

The observed lines in Ir I arise from transitions from the low even configurations $5d^76s^2$ and $5d^86s$ to the odd-parity configuration $5d^76s6p$ (Van Kleef 1957).

## 4. New experimental results

### 4.1. Radiative lifetime measurements

We have remeasured the radiative lifetimes of four levels in Os I and one level in Ir I, using the laser-induced-fluorescence (LIF) technique. A plasma cone of osmium ions and atoms was created from an osmium pellet by an ablation laser. Atoms in the expanding cone of ions were selectively photo-excited to the level under investigation by light from a pulsed tuneable dye laser, working on a red dye and pumped by a Nd:YAG laser. The dye laser light was shifted to the desired wavelengths in the near UV and deep blue using a frequency-doubling crystal and Raman shifting in a hydrogen cell. The fluorescence light due to the decay of the excited levels was then measured with a fast detection system. For levels with short lifetimes, the temporal shape of the laser pulse was also recorded, and the lifetime values were evaluated by fitting a convolution of the recorded pulse and an exponential to the fluorescence signal. The experimental set-up is described in detail by Li et al. (2000).

The general advantage of a laser produced plasma as a source of free ions and atoms is the high particle density, fairly high population in metastable levels, and the presence of high ionization stages. A major drawback is the high speed of the created particles, for neutral osmium in the range $10^3$–$10^4$ $m\,s^{-1}$. This sets an upper limit to the lifetimes that can be measured, because of flight-out-of-view effects. Possible systematic errors due to these effects were checked by changing the position of the slit of the detecting monochromator. Another test was to make lifetime recordings for different delays between the ablation laser pulse and the excitation laser pulse, thus isolating ions travelling with different velocities.

Based on these tests, we decided that our data for the $5d^66s(^6D)6p\ z\ ^7D_5$ level of Os I (lifetime ~800 ns) and the $5d^76s(^5F)6p\ z\ ^6D_{9/2}$ level of Ir I (lifetime 580 ns) were not sufficiently accurate to merit publication, and we have retained the values found by Kwiatkowski et al. (1984) and Gough et al. (1983), respectively. Kwiatkowski et al. (1984) used an oven to produce a vapour of free Os I atoms, which should lead to smaller flight-out-of-view effects than our laser ablation technique and hence to somewhat more reliable results for lifetimes in the microsecond range. A similar case is the upper level of the line at 4420 Å, which was not measured by Kwiatkowski et al. (1984) and for which no recent lifetime measurement is thus available.

Residual experimental uncertainties are divided equally between random scatter between different recordings and such possible systematic effects. There is, indeed, a direct trade-off between these two types of error: the photon shot noise in the individual recordings may be reduced by increasing the power of the ablation laser pulse or reducing the delay between the ablation and exciting laser pulses. Both of these remedies result in a denser plasma and higher light intensity at the moment of excitation, hence in an increased photon flux. The penalty for this gain is an increased component of collisional de-excitation, immediately visible as a systematic reduction of the measured lifetime.

Our final experimental results are given in Tables 1 and 2 and compared with the earlier laboratory data. In most cases the

agreement is very good. For further comparison, the lifetimes computed theoretically in Sect. 5 are also given.

### 4.2. Branching fractions

Spectra of osmium and iridium were recorded with a Chelsea Instruments FT500 UV Fourier Transform Spectrometer (FTS) in the wavelength region 2500 to 7000 Å. For osmium, a commercial hollow cathode lamp was used as the light source due to the toxic nature of osmium oxide. This sealed lamp is manufactured by ISTC, USA, and contains neon as the carrier gas. The recommended maximum operating current is 20 mA, far below the values used for our home-made hollow cathode lamps, one of which was used for iridium. The iridium light source was a water-cooled hollow-cathode lamp where the cathode consists of a 50 mm long iron cylinder with a diameter of 10 mm. A piece of iridium foil was folded and inserted into the iron cylinder. Pure neon or argon or a mixture of the two were used as carrier gases for iridium, with a discharge current between 200 and 700 mA.

The observable quantity from which branching fractions are derived is the line intensity (in photons $\text{Å}^{-1}$ $\text{s}^{-1}$). In order to obtain accurate relative intensities for lines in different wavelength regions, the recorded spectra must be corrected for the instrumental response. This was done in two different ways for different spectral regions. In the region 2500 to 5300 Å we used Ar II lines with known branching ratios (BR) (Whaling et al. 1993), produced in an Fe-Ar hollow cathode lamp run at a pressure of 0.7 torr Ar and a current of 0.3 A. In the wavelength region 4100 to 7000 Å we used a tungsten ribbon lamp with calibrated spectral energy distribution. The uncertainty in the calibration derived from known Ar II branching ratios is estimated to be 10%. The uncertainty of the tungsten lamp calibration data is 3%, and the recorded spectrum from the lamp is reproducible within 5%.

The intensity of strong transitions involving the ground state could be affected by self absorption in the laboratory light source. In order to check for any systematic errors from this effect, we investigated the intensity ratio of pairs of lines of different strength from the same upper level as a function of the discharge current through the lamp. This method is discussed in more detail by Sikström et al. (2002). None of the measured Os I or Ir I lines showed any effect of self absorption.

Finally, in order to determine the branching fractions (BFs) for a given upper level, the relative intensities for all possible downward transitions from that level must be known. These intensities were estimated by means of theoretical atomic structure calculations (see Sect. 5). The final BFs for all measured lines are given in Tables 3 and 4.

### 4.3. Wavelengths

The previous extensive analyses of Os I (Van Kleef 1957) and Ir I (Van Kleef & Klinkenberg 1961) were based on arc spectra in the wavelength region 2350 to 4850 Å. The resulting wavelengths have uncertainties of about 50 mÅ. Our FTS spectra of the hollow cathode lamp from 2500 to 7000 Å (14 300–40 000 $\text{cm}^{-1}$) are recorded at a spectral resolution of about 0.05 $\text{cm}^{-1}$ ($\lambda/\Delta\lambda \simeq 5 \times 10^5$ and $\Delta\lambda \sim 8$ mÅ at 4000 Å). The linear wavenumber scale was calibrated using Fe II lines with very accurately measured wavelengths.

Most of the Os I and Ir I lines are unresolved blends due to isotope shift and hyperfine structure (see Figs. 1 and 2), and we have determined improved centre-of-gravity wavelengths for all transitions studied in this work. The air wavelengths in Tables 3 and 4 were obtained from wavenumbers using the Edlén formula (Edlén 1966). The uncertainty in the wavenumbers is estimated to vary from 0.003 $\text{cm}^{-1}$ to 0.01 $\text{cm}^{-1}$, depending on the S/N ratio of the observation of each individual line. The wavelength uncertainty for the strong lines around 3000 Å in Table 5 is thus smaller than 1 mÅ, whereas the uncertainty for the weak lines around 5000 Å is about 2–3 mÅ.

## 5. Theoretical atomic structure calculations

The branching fractions (BFs) for individual transitions from a given upper level can be computed from the observed spectral line intensities if the relative intensities for *all* transitions from that level are known. However, some of these transitions may be too weak to be detected, and some may appear outside the observed spectral region. Therefore, we have performed atomic structure calculations, using the Cowan code (Cowan 1981), allowing us to estimate the total branching fraction of the missing lines (i.e. the residual).

For osmium we included the odd parity configurations $5d^6 6s 6p$, $5d^5 6s^2 6p$ and $5d^7 6p$ and the low even group $5d^6 6s^2$, $5d^7 6s$, and $5d^8$. Whereas the low even levels have been studied before (Kröger et al. 2002; Gluck et al. 1964), we are not aware of any earlier theoretical analysis of the odd parity levels. In advance of a revised description of Os I, it is noted that some odd parity levels have not been confirmed in the fitting process using the Cowan code (Cowan 1981). For example no $J = 7$ level is expected below 43 000 $\text{cm}^{-1}$, which leads to rejection of the 40 036 $\text{cm}^{-1}$ value. In return, the $5d^6(^3\text{H})6s6p\ ^5\text{H}_7$ level was found at 43 263.61 $\text{cm}^{-1}$ from the lines at 3518.722, 5250.463 and 5934.049 Å.

For iridium the corresponding odd parity configurations $5d^7 6s 6p$, $5d^6 6s^2 6p$, $5d^8 6p$ and even parity configurations $5d^7 6s^2$, $5d^8 6s$ and $5d^9$ were included. The calculations reproduce the observed BRs to satisfactory accuracy, presented in Tables 3 and 4, and should thus give a reasonable estimate of the sum of the omitted branches, identified as *residual* in Tables 3 and 4, provided their sum is small compared to the relative intensities of the measured lines (Sikström et al. 2002), as is clearly the case here.

A straight application of the RCG/RCE codes (Cowan 1981) provides estimated $\log(gf)$ values for the transitions included in the calculations. They show systematic deviations from the experimental values, but differing for the different types of transition. Inasmuch as the validity of the fine structure study is confirmed by the good agreement between the theoretical and experimental Landé factors, the present work suggests that a proper scaling might be applied to the dipole transition integrals derived from the HFR method as it is done from the

**Table 3.** New Os I lifetimes, wavelengths, branching fractions, and transition probabilities.

| Upper level lifetime | Lower level | $\sigma$ (cm$^{-1}$) | $\lambda_{air}$ (Å) | $BF_{exp.}$ | $BF_{th.}$ | $A_{ik}$ ($10^6$ s$^{-1}$) | Unc. (%) |
|---|---|---|---|---|---|---|---|
| $5d^5 6s^2(^6S)6p\ z\ ^7P_4$ | $5d^6 6s^2\ a^5D_4$ | 28 331.736 | 3528.602 | 0.287 | 0.306 | 1.08 | 11 |
| $\tau$ = 265.0 ns | $5d^6 6s^2\ a^5D_3$ | 24 172.410 | 4135.781 | 0.515 | 0.651 | 1.94 | 9 |
| | $5d^7(^4F)6s\ a^5F_5$ | 23 187.833 | 4311.393 | 0.195 | 0.025 | 0.73 | 11 |
| | $5d^7(^4F)6s\ a^5F_4$ | 19 187.948 | 5103.497 | 0.002 | 0.016 | 0.01 | 13 |
| | *Residual* | | | 0.001 | | | |
| $5d^6 6s(^6D)6p\ z\ ^7F_5$ | $5d^6 6s^2\ a^5D_4$ | 30 279.921 | 3301.567 | 0.935 | 0.857 | 10.05 | 7 |
| $\tau$ = 93.0 ns | $5d^7(^4F)6s\ a^5F_5$ | 25 136.049 | 3977.225 | 0.061 | 0.141 | 0.66 | 16 |
| | $5d^7(^4F)6s\ a^5F_4$ | 21 537.179 | 4641.833 | 0.003 | 0.001 | 0.03 | 17 |
| | *Residual* | | | 0.001 | | | |
| $5d^6 6s(^6D)6p\ z\ ^7F_4$ | $5d^6 6s^2\ a^5D_4$ | 32 684.629 | 3058.652 | 0.883 | 0.455 | 31.53 | 7 |
| $\tau$ = 28.0 ns | $5d^6 6s^2\ a^5D_3$ | 28 525.263 | 3504.662 | 0.044 | 0.513 | 1.57 | 13 |
| | $5d^7(^4F)6s\ a^5F_5$ | 27 540.672 | 3629.958 | 0.002 | 0.001 | 0.08 | 14 |
| | $5d^7(^4F)6s\ a^5F_4$ | 23 941.834 | 4175.612 | 0.042 | 0.023 | 1.51 | 13 |
| | $5d^7(^4F)6s\ a^3F_4$ | 21 654.104 | 4616.769 | 0.017 | 0.001 | 0.60 | 14 |
| | $5d^7(^4F)6s\ a^5F_3$ | 21 306.652 | 4692.056 | 0.007 | 0.002 | 0.25 | 14 |
| | *Residual* | | | 0.004 | | | |
| $5d^6 6s(^6D)6p\ z\ ^5F_5$ | $5d^6 6s^2\ a^5D_4$ | 34 365.335 | 2909.057 | 0.978 | 0.926 | 40.77 | 7 |
| $\tau$ = 28.0 ns | $5d^7(^4F)6s\ a^5F_5$ | 29 221.472 | 3421.160 | 0.003 | 0.066 | 0.14 | 17 |
| | $5d^7(^4F)6s\ a^5F_4$ | 25 622.608 | 3901.698 | 0.007 | 0.006 | 0.28 | 17 |
| | $5d^7(^4F)6s\ a^3F_4$ | 23 334.750 | 4284.248 | 0.010 | <0.001 | 0.40 | 17 |
| | *Residual* | | | 0.002 | | | |
| $5d^6 6s(^6D)6p\ z\ ^7D_4$ [a] | $5d^6 6s^2\ a^5D_4$ | 22 615.656 | 4420.474 | 0.988 | 0.983 | | |
| | $5d^6 6s^2\ a^5D_3$ | 18 456.293 | 5416.700 | 0.001 | 0.001 | | |
| | $5d^7(^4F)6s\ a^5F_5$ | 17 471.770 | 5721.931 | 0.008 | 0.012 | | |
| | *Residual* | | | 0.004 | | | |
| $5d^6 6s(^6D)6p\ z\ ^7D_5$ | $5d^6 6s^2\ a^5D_4$ | 23 462.896 | 4260.849 | 0.992 | 0.992 | 1.24 | 9 |
| $\tau$ = 800(70)[b] ns | *Residual* | | | 0.008 | | | |

[a] No experimental lifetime available.
[b] Lifetime measurements by Kwiatkowski et al. (1984).

**Table 4.** New Ir I lifetimes, wavelengths, branching fractions, and transition probabilities.

| Upper level lifetime | Lower level | $\sigma$ (cm$^{-1}$) | $\lambda_{air}$ (Å) | $BF_{exp.}$ | $BF_{th.}$ | $A_{ik}$ ($10^6$ s$^{-1}$) | Unc. (%) |
|---|---|---|---|---|---|---|---|
| $5d^7 6s(^5F)6p\ z\ ^6F_{11/2}$ | $5d^7 6s^2\ a^4F_{9/2}$ | 28 452.318 | 3513.647 | 0.892 | 0.973 | 2.79 | 9 |
| $\tau$ = 320 ns | $5d^8(^3F)6s\ b^4F_{9/2}$ | 25 617.333 | 3902.501 | 0.107 | 0.026 | 0.33 | 11 |
| | *Residual* | | | 0.001 | | | |
| $5d^7 6s(^5F)6p\ z\ ^6D_{9/2}$ | $5d^7 6s^2\ a^4F_{9/2}$ | 26 307.462 | 3800.124 | 0.965 | 0.996 | 1.67 | 2 |
| $\tau$ = 580[a] ns | $5d^8(^3F)6s\ b^4F_{9/2}$ | 23 472.485 | 4259.108 | 0.031 | 0.001 | 0.05 | 7 |
| | *Residual* | | | 0.001 | | | |

[a] Lifetime measurements by Gough et al. (1983).

electrostatic and spin-orbital radial integrals in the parameter fitting process.

## 6. Oscillator strengths for Os I and Ir I

### 6.1. Derivation of the gf-values

By combining the radiative lifetime ($\tau$) and the BF one can derive the transition probability ($A$-values) for lines from a particular upper level ($i$) through the relation:

$$A_{ik} = \frac{BF_{ik}}{\tau_i}. \quad (1)$$

Experimental BFs and $A$-values are presented in Table 3 (using the Os I lifetime measurement by Kwiatkowski et al. 1984), and Table 4. The $A$-values can be converted to oscillator strengths or $gf$-values by

$$gf = 1.4992 \times 10^{-16} \lambda^2 g_u A, \quad (2)$$

where $\lambda$ is in Å, $A$ in s$^{-1}$, and $g_u$ and $g$ are the statistical weights for the upper and lower levels, respectively. The log($gf$) values for the investigated transitions are presented in Table 5.

Uncertainties for the $A$-values are quoted in Tables 3 and 4. The method by which the uncertainties are determined is

**Table 5.** Finding list of new experimental log($gf$)-values for the Os I and Ir I transitions in Tables 3 and 4.

| $\lambda_{air}$ (Å) | Transition | log($gf$) Exp | Unc.[a] | Kurucz |
|---|---|---|---|---|
| | Os I | | | |
| 2909.057 | $5d^6 6s^2\ a^5D_4 - 5d^6 6s(^6D)6p\ z^5F_5$ | –0.25 | 7 | –0.32[b] |
| 3058.652 | $5d^6 6s^2\ a^5D_4 - 5d^6 6s(^6D)6p\ z^7F_4$ | –0.45 | 7 | –0.43[c] |
| 3301.567 | $5d^6 6s^2\ a^5D_4 - 5d^6 6s(^6D)6p\ z^7F_5$ | –0.74 | 7 | –0.75[c] |
| 3421.160 | $5d^7(^4F)6s\ a^5F_5 - 5d^6 6s(^6D)6p\ z^5F_5$ | –2.57 | 17 | –1.33[b] |
| 3504.662 | $5d^6 6s^2\ a^5D_3 - 5d^6 6s(^6D)6p\ z^7F_4$ | –1.64 | 13 | –1.39[c] |
| 3528.602 | $5d^6 6s^2\ a^5D_4 - 5d^5 6s^2(^6S)6p\ z^7P_4$ | –1.74 | 11 | |
| 3629.958 | $5d^7(^4F)6s\ a^5F_5 - 5d^6 6s(^6D)6p\ z^7F_4$ | –2.91 | 14 | –2.32[c] |
| 3901.698 | $5d^7(^4F)6s\ a^5F_4 - 5d^6 6s(^6D)6p\ z^5F_5$ | –2.15 | 17 | –1.66[b] |
| 3977.225 | $5d^7(^4F)6s\ a^5F_5 - 5d^6 6s(^6D)6p\ z^7F_5$ | –1.77 | 17 | –1.43[b] |
| 4135.781 | $5d^6 6s^2\ a^5D_3 - 5d^5 6s^2(^6S)6p\ z^7P_4$ | –1.35 | 9 | –1.26[c] |
| 4175.612 | $5d^7(^4F)6s\ a^5F_4 - 5d^6 6s(^6D)6p\ z^7F_4$ | –1.50 | 13 | –1.24[c] |
| 4260.849 | $5d^6 6s^2\ a^5D_4 - 5d^6 6s(^6D)6p\ z^7D_5$ | –1.47 | 9 | –1.44[c] |
| 4284.248 | $5d^7(^4F)6s\ a^3F_4 - 5d^6 6s(^6D)6p\ z^5F_5$ | –1.91 | 17 | –1.67[c] |
| 4311.393 | $5d^7(^4F)6s\ a^5F_5 - 5d^5 6s^2(^6S)6p\ z^7P_4$ | –1.74 | 11 | –1.85[c] |
| 4616.769 | $5d^7(^4F)6s\ a^3F_4 - 5d^6 6s(^6D)6p\ z^7F_4$ | –1.82 | 14 | –1.67[c] |
| 4641.833 | $5d^7(^4F)6s\ a^5F_4 - 5d^6 6s(^6D)6p\ z^7F_5$ | –2.96 | 14 | –2.73[c] |
| 4692.056 | $5d^7(^4F)6s\ a^5F_3 - 5d^6 6s(^6D)6p\ z^7F_4$ | –2.18 | 14 | –2.05[c] |
| 5103.497 | $5d^7(^4F)6s\ a^5F_4 - 5d^5 6s^2(^6S)6p\ z^7P_4$ | –3.50 | 13 | –2.43[c] |
| | Ir I | | | |
| 3513.647 | $5d^7 6s^2\ a^4F_{9/2} - 5d^7 6s(^5F)6p\ z^6F_{11/2}$ | –1.246 | 9 | –1.260[b] |
| 3800.124 | $5d^7 6s^2\ a^4F_{9/2} - 5d^7 6s(^5F)6p\ z^6D_{9/2}$ | –1.489 | 2 | –1.450[b] |
| 3902.501 | $5d^8(^3F)6s\ b^4F_{9/2} - 5d^7 6s(^5F)6p\ z^6F_{11/2}$ | –2.077 | 11 | –1.930[b] |
| 4259.108 | $5d^8(^3F)6s\ b^4F_{9/2} - 5d^7 6s(^5F)6p\ z^6D_{9/2}$ | –2.882 | 7 | –2.900[b] |

[a] One-$\sigma$ uncertainty of $gf$, in %.
[b] Experimental values rescaled by Kurucz (Kurucz 1993).
[c] Unscaled values from Kwiatkowski et al. (1984).

described by Sikström et al. (2002). For the lifetime measurements the uncertainties are of the order of 7–8%, and the uncertainties in the BFs based on the intensity measurements range from 1% for strong lines to 10% for weak lines. The small residuals introduce very small errors in the final BFs, even though there is a discrepancy between calculated and theoretical lifetimes in Tables 1 and 2. However, there is no need to rescale the theoretical lifetimes in the calculations of the BFs for the missing lines.

For comparison with our new results, the older experimental values of log($gf$) by Kurucz (1993) are given in the last column of Table 5.

### 6.2. Comparison with earlier results

We have compared our new experimental log($gf$) values with the earlier data by Kurucz (1993), which are those used to derive abundances of Os I and Ir I in the very metal-poor, *r*-process enriched halo giants. Figure 3 shows the result of this comparison for Os I. As seen, there is good agreement between the experimental results for the three strongest lines ($\Delta\log(gf) = -0.020 \pm 0.049$ ($1\sigma$)). However, already for the four lines with log($gf$) near −1.5 (including those used for stellar abundance determinations in the optical region) is there substantial disagreement ($\Delta\log(gf) = +0.156 \pm 0.114$ ($1\sigma$)), and for the weaker lines both the offset and the dispersion increase even further. The sense of these deviations is such as to suggest the presence of systematic calibration errors in the spectra used to derive the earlier branching fractions. Similar comments

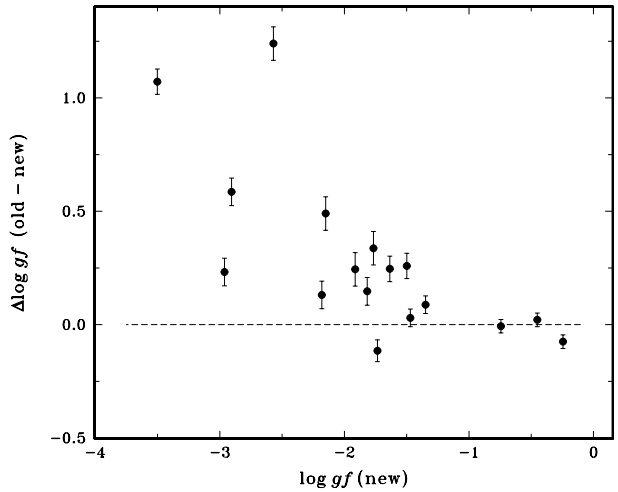


**Fig. 3.** The differences between old and new experimental log($gf$) values, plotted as a function of log($gf$) for the Os I lines in Table 5. Error bars indicate the uncertainties of our new values.

apply to the comparison with the theoretical results, except that the scatter is even larger.

For Ir I the new and previous experimental data are in excellent agreement ($\Delta \log(gf) = +0.014 \pm 0.034(1\sigma)$). The $\log(gf)$ values for the Ir I lines of greatest astrophysical importance thus appear to be well-established despite the relatively large scatter of the theoretical computations.

## 7. Discussion

### 7.1. Os and Ir abundances in metal-poor stars

In *r*-process enriched, very metal-poor stars, the heavy neutron capture elements with $Z \geq 56$ follow the solar *r*-process abundance pattern, scaled according to the overall neutron-capture element content of the star (Truran et al. 2002). In particular, the third *r*-process peak elements Os and Ir also generally conform to the same solar *r*-process abundance pattern as the elements with $56 \leq Z \leq 68$ (Truran et al. 2002). However, the results of Hill et al. (2002) for CS 31082-001 suggested that the Os abundance might somewhat exceed the scaled solar *r*-process value in this star. Given that the actinides ($Z \geq 80$) are significantly overabundant in CS 31082-001 with respect to the lower-mass *r*-process elements (by a factor ∼2.5, or 0.4 dex), the question arises whether Os is also overabundant in a similar manner. If so, the overabundance of the actinides might extend to lower-mass nuclides, and Os would potentially be a useful stable reference element with which to measure the radioactive decay of U and Th.

Our $\log(gf)$ remeasurements confirm and consolidate the conclusion that Ir conforms closely to the solar *r*-process abundance pattern as scaled to match the elements with $56 \leq Z \leq 68$. For Os I, however, the small number of lines used in previous abundance determinations and their relatively poor consistency justify a re-evaluation of the few stellar Os detections in the literature in the light of our new $\log(gf)$ values.

So far, Os has been detected in five metal-poor stars: HD 115444 and HD 126238 (Sneden et al. 1998), CS 22892-052 (Sneden et al. 2003), BD+17°3248 (Cowan et al. 2002) and CS 31082-001 (Hill et al. 2002). In the first two stars, the determination is based on two UV lines only ($\lambda\lambda$ 2838 and 3058 Å) observed with HST, one of which is included in the present study (3058 Å). Our $\log(gf)$ revisions have negligible effect (0.021 dex) on the abundance of Os in these two stars. The Os abundances of CS 22892-052 and BD+17°3248 are based on a mix of UV (HST spectra) and near-UV (Keck and VLT spectra), for a total of 4 lines in the former and 5 in the latter star, of which 3 lines are also included in the present study. Our $\log(gf)$ corrections also cause negligible revision of the Os abundance in these two stars (+0.013 and 0.003 respectively).

The Os abundance in CS 31082-001 is, however, so far based on only 3 lines in the visible region ($\lambda\lambda$ 4135, 4261, and 4420 Å), for which the $\log(gf)$ values have been revised significantly (−0.03 dex and −0.07 for the first two lines, respectively). Given the double interest of CS 31082-001 as one of the few very metal-poor stars in which Os and Ir have been measured, and the only one in which uranium has also been detected along with numerous lines of Th, we decided to re-examine the abundances of Os and Ir in this star, based on a larger set of newly-detected lines.

**Table 6.** Os and Ir abundances in CS 31082-001.

| $\lambda$ (Å) | Exc. pot. (eV) | $\log gf$ | $\log \epsilon^a$ |
|---|---|---|---|
| Os I | | | |
| 3058.652 | 0.00 | −0.451 | 0.15 |
| 3267.945 | 0.00 | −1.080[d] | 0.20 |
| 3269.204 | 0.715 | −1.070[c] | 0.2: |
| 3301.567 | 0.00 | −0.743 | 0.25 |
| 3504.662 | 0.52 | −1.636 | 0.2: |
| 3528.602 | 0.00 | −1.740 | 0.20 |
| 4135.775 | 0.52 | −1.260 | 0.60 |
| 4260.848 | 0.00 | −1.440 | 0.21 |
| 4420.468 | 0.00 | −1.530[d] | 0.5:[b] |
| Ir I | | | |
| 3513.648 | 0.00 | −1.246 | 0.19 |
| 3800.120 | 0.00 | −1.489 | 0.24 |

[a] Abundance in the usual notation where $\log \epsilon(\mathrm{H}) = 12$.
[b] Line heavily blended (see text).
[c] Experimental values rescaled by Kurucz (Bell heavy).
[d] Unscaled values from Kwiatkowski et al. (1984).

### 7.2. Reanalysis of Os and Ir in CS 31082-001

Since the paper by Hill et al. (2002), new VLT spectra of CS 31082-001 have been obtained including the region 3000–3100 Å at the same resolution ($R = 77\,000$) as the spectra described in Hill et al. (2002) – a tribute to the efficiency of the VLT+UVES. The co-added spectrum of CS 31082-001 was searched again for Os I and Ir I lines in the whole wavelength range now available. No new iridium features were positively detected, but 6 new Os I lines were identified in addition to the three listed by Hill et al. (2002). Among the new total of 9 Os I lines, 6 have new oscillator strengths from this paper, and we have rederived the Os abundance in CS 31082-001 from all 9 lines, using these new data. The results from the individual lines are given in Table 6, and examples of the fits to the observed spectrum are given in Fig. 4. The model atmosphere, spectral synthesis code, and stellar parameters ($T_{\rm eff}$, $\log g$, and overall metallicity) were those adopted by Hill et al. (2002).

Table 6 reveals a remarkable result: most features (7 out of 9) agree on a mean Os abundance of $\log \epsilon(\mathrm{Os}) = 0.2$ dex, to within ±0.03 dex ($1\sigma$). In contrast, two of the lines in the 4000 Å region – i.e. two of the three Os I lines most easily observable until the near-UV spectral region became accessible – stand out from the mean. As noted already by Hill et al. (2002), the 4420.468 Å line is a close blend of Os I and Sm II, and the high Os abundance derived from this feature can be reconciled with the mean of the other lines by assuming a Sm abundance 0.15 dex higher than the average from other lines (or by lowering $\log(gf)$ for the Sm line by 0.15 dex). Such a Sm abundance would be only $1\sigma$ away from the mean, so we conclude that the discrepancy for the 4420.468 Å Os line is not significant.

The 4135.775 Å feature appears to be very clean (see Fig. 4), but nevertheless gives a significantly higher Os

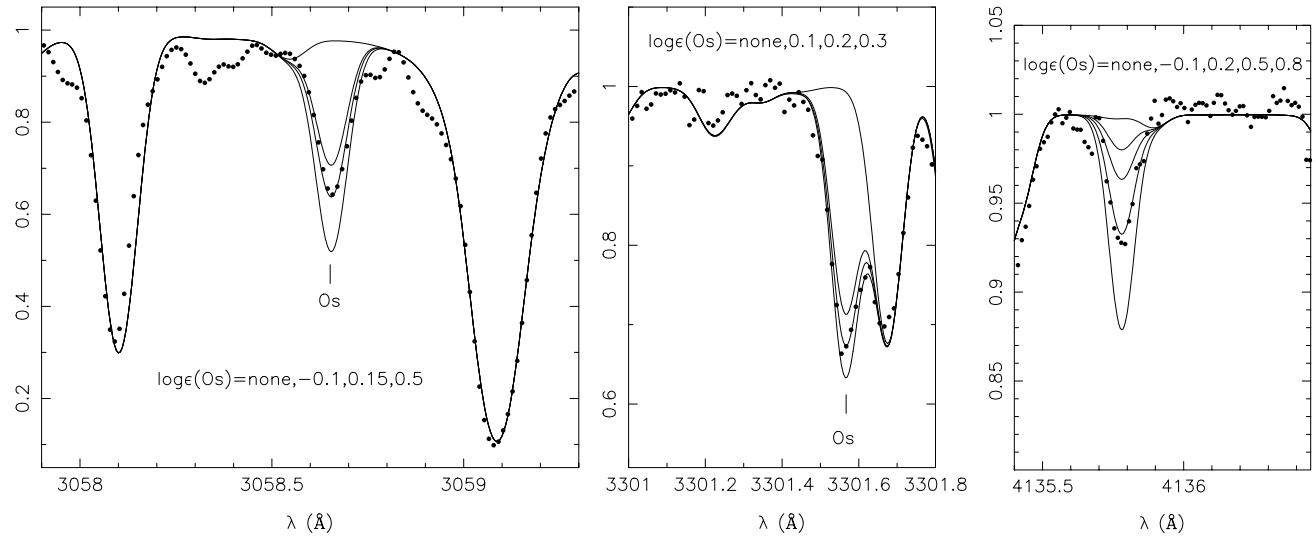


**Fig. 4.** The Os I lines at 3058, 3301 and 4135 Å in CS 31082-001. *Dots*: observed spectrum; *full lines*: synthetic spectra computed for the abundances indicated in the figure.

abundance than all the other lines (by 0.3 dex). We have searched for possible blends which might explain this, but found nothing significant: No molecular lines are expected at this wavelength, and the only atomic lines in the immediate vicinity – Fe I 4135.755 Å and Cr I 4135.829 Å – should be far too weak to influence the Os feature (even if we artifically increase their $\log(gf)$ by +0.5 dex). We therefore suggest that an *unidentified line* is superimposed on this Os I feature, making abundance determinations from it unreliable.

The final osmium abundance for CS 31082-001 is found to be $\log\epsilon = 0.22 \pm 0.08$ ($1\ \sigma$, $n = 8$), excluding the 4135.781 Å line from the mean and weighting each line by its inverse variance (: in Table 6 denotes uncertain determinations, because the features in question are faint or blended). The Ir I abundance is $\log\epsilon = 0.22 \pm 0.04$ ($1\ \sigma$, $n = 2$), essentially identical to the value by Hill et al. (2002) and now also to that of Os.

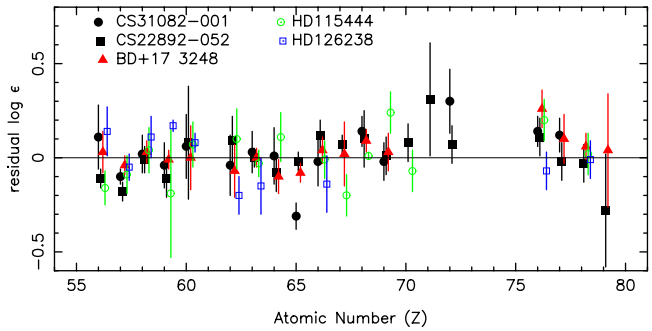


**Fig. 5.** Abundance residuals of the heavy elements in five metal-poor stars (see text) from the solar-system *r*-process pattern (Arlandini et al. 1999). The normalisation was computed as the mean difference between the solar-system *r*-process and the stellar abundances for each star in the range $56 \le Z \le 79$. The symbols for the different stars have been shifted horizontally in steps of 0.1 to enhance readability.

## 8. Conclusions

The revised Os abundance of CS 31082-001 not only agrees with that of Ir in this star, but results in agreement between the observed heavy-element abundances and the scaled solar *r*-process in the *whole mass range* $56 \le Z \le 79$ (see Fig. 5). Moreover, this now holds in all five very metal-poor stars with measured Os and Ir abundances. From a theoretical point of view it was a puzzle that Os appeared to deviate from the solar *r*-process pattern, because the quite different neutron-capture scenarios described by Schatz et al. (2002) and Wanajo et al. (2002) show little if any differences in the production of Os and Ir. Accordingly, the apparent overabundance of Os was hard to understand when not accompanied by a similar effect for Ir. On the other hand, the same models show that under certain conditions the actinides *can* be overproduced relative to even such nearby elements as Os and Ir (see Wanajo et al. 2002).

Within the limitations of the small sample (only 5 stars so far), these results would appear to establish that (i): reliable Os abundances can be determined from the UV lines and $\lambda$4260 Å, but not from $\lambda\lambda$4135, 4420 Å until their blending problems have been resolved; (ii): the abundances of Os and Ir are identical in all observed stars; (iii): the observed heavy-element abundances in very metal-poor stars agree precisely with the scaled solar *r*-process pattern in the entire mass range $56 \le Z \le 79$; and (iv): neither Os or Ir nor any lighter elements can be used as stable references from which to measure the radioactive decay of Th and U in such stars.

Accordingly, reliable abundances for elements between Ir and Th (notably Pt, Bi, and Pb) in CS 31082-001 and similar stars are needed to further constrain the models of *r*-process nucleosynthesis. The exact atomic mass at which overproduction may set in for the heaviest *r*-process elements, including at least the actinides, is of special interest. Equally important are the daughter elements Pb and Bi of the decay of Th and U, as constraints on the original amounts of the parent nuclides as well as any amounts of Pb and Bi that might have been produced by other means. We note in this context that Pb appears to be below even the small solar *r*-process

fraction in both CS 22892-052 and CS 31082-001 (Hill et al. 2002; Sneden et al. 2003). This requires high-quality spectra in the ultraviolet region beyond the atmospheric cutoff, which we are currently obtaining with the *Hubble Space Telescope*. In addition to the Pt, Bi, and Pb abundances, these spectra will allow an independent check of the Os I abundance from the three strong deep-UV lines with well-determined $\log(gf)$ values (see Table 5).

*Acknowledgements.* We gratefully acknowledge the excellent conditions at the Lund Laser Centre and the support by its Director, Prof. Sune Svanberg, for this research, which also received financial support from the European Community under the Programme "Improving Human Potential – Access to Research Infrastructures" (Contract No. HPRI-CT-1999-00041). Additional support was received from grants by the Swedish Research Council (to S.J. and B.N.) and the Nordic Academy for Advanced Study (NorFA; to B.N). The ESO-VLT observations of CS 31082-001 were made in the framework of the *Large Programme* "First Stars" (165.N-0276(A); P.I. R. Cayrel).

## References

Arlandini, C., Käppeler, F., Wisshak, K., et al. 1999, ApJ, 525, 886
Cayrel, R., Hill, V., Beers, T. C., et al. 2001, Nature, 409, 691
Corliss, C. H., & Bozman, W. R. 1962, NBS Monograph, 53
Cowan, J. J., Sneden, C., Burles, S., et al. 2002, ApJ, 572, 861
Cowan, R. D. 1981, The Theory of Atomic Structure and Spectra (Berkley: Univ. of California Press)
Edlén, B. 1966, Metrologia, 2, 71
Gluck, G., Bordarier, Y., Bauche, J., & van Kleef, T. A. M. 1964, Physica, 30, 2068
Gough, D. S., Hannaford, P., & Lowe, R. M. 1983, J. Phys. B, 16, 785
Hill, V., Plez, B., Cayrel, R., et al. 2002, A&A, 387, 560
Johnson, J., & Bolte, M. 2002, ApJ, 579, 616
Kröger, S., Basar, G., Baier, A., & Guthöhrlein, H. G. 2002, Phys. Scr., 65, 56
Kurucz, R. L. 1993, Synthesis Programs and Line Data (Kurucz CD-ROM No. 18)
Kwiatkowski, M., Zimmermann, P., Biémont, E., & Grevesse, N. 1984, A&A, 135, 59
Li, Z. S., Lundberg, H., Wahlgren, G. M., & Sikström, C. M. 2000, Phys. Rev A, 62, 032505
Sawatzky, G., & Winkler, R. 1989, Z. Phys. D, 14, 9
Schatz H., Toenjes R., Pfeiffer B., et al. 2002, ApJ, 579, 626
Sikström, C. M., Nilsson, H., Litzén, U., Blom, A., & Lundberg, H. 2002, J. Quant. Spectrosc. Radiat. Trans., 74, 355
Sneden, C., Cowan, J. J., Burris, D. L., & Truran, J. W. 1998, ApJ, 496, 235
Sneden, C., Cowan, J. J., Lawler, J. E., et al. 2003, ApJ, 591, 936
Sneden, C., McWilliam, A., Preston, G. W., et al. 1996, ApJ, 467, 819
Truran, J. W., Cowan, J. J., Pilachowski, C. A., & Sneden, C. 2002, PASP, 114, 1293
Van Kleef, T. A. M. 1957, Physica, 23, 843
Van Kleef, T. A. M., & Klinkenberg, P. F. A. 1961, Physica, 27, 83
Wanajo, W., Itoh, N., Ishimaru, Y., Nozawa, S., & Beers, T. C. 2002, ApJ, 577, 853
Whaling, W., Carle, M. T., & Pitt, M. L. 1993, J. Quant. Spectrosc. Radiat. Trans., 50, 7